J. Fluid Mech. (1998), *vol.* 372, *pp.* 71–91. Printed in the United Kingdom

Weakly nonlinear shear waves

By FALK FEDDERSEN

Center for Coastal Studies, Scripps Institution of Oceanography, University of California, San Diego, La Jolla, CA 92093-0209, USA

(Received 26 August 1997 and in revised form 11 May 1998)

Alongshore propagating low-frequency $O(0.01$ Hz) waves related to the direction and intensity of the alongshore current were first observed in the surf zone by Oltman-Shay, Howd & Birkemeier (1989). Based on a linear stability analysis, Bowen & Holman (1989) demonstrated that a shear instability of the alongshore current gives rise to alongshore propagating shear (vorticity) waves. The fully nonlinear dynamics of finite-amplitude shear waves, investigated numerically by Allen, Newberger & Holman (1996), depend on α, the non-dimensional ratio of frictional to nonlinear terms, essentially an inverse Reynolds number. A wide range of shear wave environments are reported as a function of α, from equilibrated waves at larger α to fully turbulent flow at smaller α. When α is above the critical level α_c, the system is stable. In this paper, a weakly nonlinear theory, applicable to α just below α_c, is developed. The amplitude of the instability is governed by a complex Ginzburg–Landau equation. For the same beach slope and base-state alongshore current used in Allen *et al.* (1996), an equilibrated shear wave is found analytically. The finite-amplitude behaviour of the analytic shear wave, including a forced second-harmonic correction to the mean alongshore current, and amplitude dispersion, agree well with the numerical results of Allen *et al.* (1996). Limitations in their numerical model prevent the development of a side-band instability. The stability of the equilibrated shear wave is demonstrated analytically. The analytical results confirm that the Allen *et al.* (1996) model correctly reproduces many important features of weakly nonlinear shear waves.

1. Introduction

Low-frequency approximately non-dispersive alongshore propagating waves with periods of $O(100$ s) and wavelengths of $O(100$ m) were first observed on a barred beach by Oltman-Shay, Howd & Birkemeier (1989). The wavelengths of these motions are much shorter than the wavelengths of edge waves of the same frequency, and are related to the intensity and direction of the mean alongshore current. In a companion paper, Bowen & Holman (1989) used linear stability theory, an idealized topography, and an idealized alongshore current to demonstrate that a shear instability of the alongshore current leads to growing, nearly non-dispersive shear waves propagating in the direction of the alongshore current. Dodd, Oltman-Shay & Thornton (1992) included a linearized bottom stress, realistic barred-beach profile, and alongshore currents, and found good agreement between wavelengths and frequencies of the most unstable linear mode and the energetic regions of the observed frequency–wavenumber spectra of velocity. However, neither linear stability analyses nor frequency–wavenumber spectra address the finite-amplitude behaviour of shear waves.

The finite-amplitude behaviour of shear waves was investigated numerically by

Allen, Newberger & Holman (1996, hereafter ANH96). Using the rigid-lid shallow-water equations on a planar beach with an idealized alongshore forcing and a linearized bottom stress, ANH96 found that the nonlinearity of the flow can be characterized by a non-dimensional parameter α (Q in ANH96), the ratio of frictional to nonlinear terms, essentially an inverse Reynolds number. For values of α below the critical value for an instability α_c, a wide range of behaviour is reported, ranging from steady equilibrated waves at larger values of α to irregular eddies and transient rips at smaller values of α. In ANH96, shear wave energy propagates non-dispersively for all values of α. It is not known whether natural shear wave environments are similar to those at larger or smaller α reported by ANH96.

ANH96 did not study the near critical (i.e. at α just below α_c) behaviour of shear waves. An issue complicating such study is that numerical effects can alter the near critical behaviour. For example, Hyman, Nicolaenko & Zaleski (1986) found that inadequate numerical accuracy could induce a false stability in simulations of the Kuramoto–Sivashinsky equation. In the ANH96 model, finite numerical resolution and biharmonic friction (added for numerical stability) might significantly distort the solutions near α_c. Note also that finite alongshore domain lengths prevent potential side-band instabilities and motions on scales longer than the domain length from developing.

In this paper analytic shear wave solutions are found for near critical conditions when the departure from stability, given by ϵ

$$\epsilon^2 = \frac{\alpha_c - \alpha}{\alpha_c}, \tag{1.1}$$

is small that largely confirm the results of ANH96. Preliminary work on the finite-amplitude weakly nonlinear theory has been reported by Dodd & Thornton (1992). Recently Shrira, Voronovich & Kozhelupova (1997) demonstrated that, for weak bottom friction ($\alpha \ll 1$), resonant triads composed of growing waves experience an explosive instability. Here we follow the approach of Stewartson & Stuart (1971), who solved for the finite-amplitude behaviour of instabilities of plane Poiseulle flow. An equation for the perturbation potential vorticity is derived in terms of the perturbation streamfunction ψ, and expanded in powers of ϵ. At $O(\epsilon)$ (e.g. Bowen & Holman 1989; Dodd *et al.* 1992), the eigenvalue problem for ψ at a particular α and alongshore wavenumber k yields growing or decaying alongshore propagating wave solutions for the streamfunction. There is a critical pair (α_c, k_c) such that one eigenvalue has zero imaginary component whose eigenfunction is a neutrally stable wave, and the rest have negative imaginary components whose eigenfunctions are decaying solutions. The frequency of the neutrally stable mode is by definition the primary frequency. At $O(\epsilon^2)$ phenomena typical of weakly nonlinear waves are found: a correction to the mean flow and a forced wave (second harmonic) at twice the primary frequency and wavenumber. At $O(\epsilon^3)$ the complex Ginzburg–Landau equation for the amplitude of the disturbance is derived. This equation has solutions that can exhibit a wide variety of behaviour ranging from a simple steady wave to chaotic solutions (Manneville 1990). For the same choice of beach slope and alongshore forcing as ANH96, the real part of the Landau coefficient is negative, indicating that the instability is supercritical and that equilibrated finite-amplitude solutions are possible at $O(\epsilon^3)$. Time-periodic solutions for the amplitude of the disturbance are side-band stable, and amplitude dispersion, a frequency shift of the equilibrated wave related to ϵ, is found.

Analytic solutions are compared to numerical solutions using the model of ANH96 at α near α_c. Equilibrated finite-amplitude waves are found in the ANH96 solutions,

and exhibit characteristic features of weakly nonlinear systems, such as spectral peaks at integer frequencies of the primary frequency and amplitude dispersion. Numerical effects that affect the near critical behaviour of the shear instability also complicate comparison with the analytic model, particularly since α_c for the ANH96 model is different from the analytic model. Nevertheless, the cross-shore structures of the ANH96 model primary wave, the second harmonic, and the mean flow correction are in excellent agreement with theory. Although differences in the α_c and therefore the ϵ of the two models prevent quantitative comparison of shear wave amplitudes, the ANH96 model shear wave amplitudes and amplitude dispersion are in reasonable agreement with the analytic model. The overall level of agreement between the analytic and ANH96 model verifies that the ANH96 model correctly reproduces the qualitative behaviour of weakly nonlinear shear waves.

The remainder of this paper is organized as follows. The weakly nonlinear theory for a planar beach and arbitrary background alongshore current is developed in §2. The numerical method and solutions for the finite-amplitude shear waves are described in §3. Comparisons to ANH96 are given in §4. Section 5 contains a discussion and conclusions.

2. Theory

Including forcing and linear bottom friction, the rigid-lid shallow water equations (continuity, cross- and alongshore momentum) representing the depth- and time-averaged flow in the nearshore are

$$(hu)_x + (hv)_y = 0, \tag{2.1a}$$

$$u_t + uu_x + vu_y = -g\eta_x - vu/h, \tag{2.1b}$$

$$v_t + uv_x + vv_y = -g\eta_y + F - vv/h, \tag{2.1c}$$

where x and y are the cross- and alongshore coordinates respectively (figure 1), u and v are the cross- and alongshore velocities, η is the sea surface elevation, v is a constant friction coefficient, and g represents gravity. This system of equations (2.1) is the same as in ANH96 except that biharmonic friction terms included in ANH96 to dampen numerical instabilities are not required here. The bathymetry contours are planar ($h(x) = \beta x$) and the shoreline is at $x = 0$. Following ANH96, the forcing $F(x)$ from breaking, obliquely incident, surface-gravity waves is for simplicity alongshore directed and does not vary in the alongshore direction. The bottom stress terms (e.g. vv/h) are an idealized representation of the bulk effects of bottom stress in the surf zone. This representation has the advantage that it is simple analytically, and has been used in the linear stability problem (Dodd *et al.* 1992; Falques & Iranzo 1994) and by ANH96. Although other bottom stress representations which take orbital wave velocities into account are probably more realistic in the surf zone (e.g. Thornton & Guza 1986), the simple bottom stress representation is appropriate for both numerical-model-based (e.g. ANH96) and theory-based process studies of shear waves, and allows comparison of the present results to ANH96.

If the alongshore current is steady and independent of y (i.e. $v = V(x)$), it then follows from the continuity equation and the boundary condition of no mass flux into the shoreline ($hu = 0$ at $x = 0$) that u vanishes everywhere. The base-state alongshore current whose stability will be investigated is then given by a balance between forcing

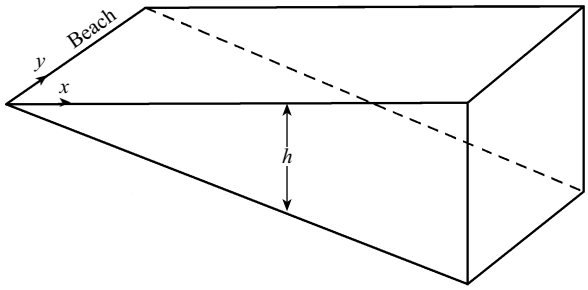

FIGURE 1. The coordinate system used: x is the cross-shore coordinate and y is the alongshore coordinate.

and bottom friction,

$$V(x) = \frac{Fh}{\nu} = \frac{F\beta x}{\nu}.$$

The shallow water equations are non-dimensionalized with the following scalings (ANH96):

$$u = Uu', \quad v = Uv', \qquad x = Lx', \quad y = Ly',$$

$$t = Tt' = \frac{L}{U}t', \qquad g\eta = N\eta',$$

$$h = h_o h' = \beta L x', \qquad F = \frac{U\nu}{h_o}F' = \frac{U\nu}{\beta L}F',$$

where the primed quantities are non-dimensional. The choice for the length scale L is typically the distance from the shoreline to the maximum in the alongshore current. Previous linear stability analyses (e.g. Putrevu & Svendsen 1992) have found that the ratio of L to the wavelength of the fastest growing wave is $O(1)$. The velocity scale U chosen is the maximum of the base-state alongshore current $V(x)$. The choice for the time scale $T = L/U$ is based on the observation (Oltman-Shay *et al.* 1989; Dodd *et al.* 1992) and linear stability result (e.g. Bowen & Holman 1989; Putrevu & Svendsen 1992) that the shear wave phase speed is 0.5–0.7 of the maximum alongshore current. Falques & Iranzo (1994) have found that the rigid-lid approximation used here is excellent for the linear stability problem when the maximum of the Froude number $Fr = V(x)/(gh(x))^{1/2}$, is 0.14, and still quite reasonable for values as large as $Fr_{max} = 0.63$. The affect of the rigid-lid approximation on finite-amplitude shear waves was investigated numerically by Özkan & Kirby (1995) whose results were quantitatively consistent with those of ANH96 with $Fr_{max} = 0.154$.

Dropping the primes, the resulting non-dimensional equations are

$$(ux)_x + (vx)_y = 0, \tag{2.2a}$$

$$u_t + uu_x + vu_y = -\gamma\eta_x - \alpha u/x, \tag{2.2b}$$

$$v_t + uv_x + vv_y = -\gamma\eta_y + \alpha(F - v/x), \tag{2.2c}$$

where $\gamma = N/U^2$ is the ratio of pressure forces to nonlinearity, and $\alpha = \nu/\beta U$ is the ratio of frictional and nonlinear terms, an inverse Reynolds number, analogous to the parameter Q of ANH96. The non-dimensional base-state alongshore current is $V(x) = xF(x)$.

Consider a perturbation of u and v about the base-state alongshore current $V(x)$.

The non-dimensional perturbation equations become

$$(ux)_x + (vx)_y = 0,$$

$$u_t + uu_x + (v+V)u_y = -\gamma\eta_x - \alpha u/x,$$

$$v_t + u(v_x + V_x) + (v+V)v_y = -\gamma\eta_y - \alpha v/x.$$

Taking the curl of the perturbation momentum equations, dividing by the water depth and substituting the continuity equation yields a perturbation potential vorticity equation

$$\frac{\mathrm{D}q}{\mathrm{D}t} + uQ_x = \frac{\alpha}{x}\left[-\left(\frac{v}{x}\right)_x + \left(\frac{u}{x}\right)_y\right],$$

where

$$\frac{\mathrm{D}}{\mathrm{D}t} = \frac{\partial}{\partial t} + u\frac{\partial}{\partial x} + (V+v)\frac{\partial}{\partial y}.$$

The perturbation potential vorticity is $q = \zeta/x$, the perturbation vorticity is $\zeta = v_x - u_y$, and the background potential vorticity is $Q = V_x/x$. In terms of the perturbation transport streamfunction ψ, where $\psi_x = xv$ and $\psi_y = -xu$, the potential vorticity becomes

$$q = \frac{1}{x^2}\left(\nabla^2\psi - \psi_x/x\right),$$

and the potential vorticity equation is

$$\frac{\mathrm{D}}{\mathrm{D}t}\left[\frac{1}{x^2}(\nabla^2\psi - \psi_x/x)\right] - \frac{\psi_y}{x}Q_x = -\frac{\alpha}{x^3}\left(\nabla^2\psi - 2\psi_x/x\right). \tag{2.3}$$

The boundary conditions of no cross-shore mass flux at both the shoreline and far offshore make ψ constant at $x = 0$ and ∞. The perturbation is assumed not to induce any net alongshore transport so ψ is the same constant (set for convenience to $\psi = 0$) at $x = 0$ and ∞. Fully expanded in terms of ψ and multiplied by x^2, (2.3) becomes

$$(\nabla^2\psi - \psi_x/x)_t - \frac{\psi_y}{x}\left(\nabla^2\psi_x - 2\nabla^2\psi/x - \psi_{xx}/x + 3\psi_x/x^2\right) - xQ_x\psi_y + \left(V + \frac{\psi_x}{x}\right)(\nabla^2\psi_y - \psi_{xy}/x) = -\frac{\alpha}{x}\left(\nabla^2\psi - 2\psi_x/x\right). \tag{2.4}$$

This equation and the boundary conditions on ψ govern the evolution of shear instabilities on a planar sloping bottom with a given base-state alongshore current. Substituting a perturbation expansion of ψ,

$$\psi = \epsilon\psi_1 + \epsilon^2\psi_2 + \epsilon^3\psi_3 + \cdots, \tag{2.5}$$

into (2.4) and collecting terms of $O(\epsilon)$ yields

$$\mathrm{L}[\psi_1] = (\nabla^2\psi_1 - \psi_{1x}/x)_t - xQ_x\psi_{1y} + V(\nabla^2\psi_{1y} - \psi_{1xy}/x) + \frac{\alpha}{x}\left(\nabla^2\psi_1 - 2\psi_{1x}/x\right) = 0. \tag{2.6}$$

This equation determines the linear stability of the flow. An alongshore propagating wave solution for ψ_1,

$$\psi_1 = \phi_1(x)\exp[\mathrm{i}k(y - ct)] + \text{c.c.},$$

is substituted into (2.6) where k is an alongshore wavenumber and c.c. denotes the complex conjugate. In general, c is complex. The real part c_r is the phase speed and

is related to the frequency of the wave by $\omega = kc_r$. The imaginary part c_i is related to the linear growth rate of the wave as $\sigma = kc_i$. Collecting terms proportional to $\exp[ik(y-ct)]$ yields (Dodd *et al.* 1992; ANH96)

$$\left(V - \frac{i\alpha}{kx} - c\right)(\phi_{1xx} - \phi_{1x}/x - k^2\phi_1) = xQ_x\phi_1 - \frac{i\alpha}{kx^2}\phi_{1x} \tag{2.7}$$

with boundary conditions $\phi_1(0) = \phi_1(\infty) = 0$. For a particular paired value of k and α, an infinite set of paired eigenvalues c and eigenfunctions $\phi_1(x)$ are solutions of (2.7). To proceed with the weakly nonlinear analysis, the critical $\alpha = \alpha_c$ is sought such that there is only one wavenumber, $k = k_c$, for which a single eigenvalue is purely real, while all others have negative imaginary parts. At all other wavenumbers the solutions decay ($c_i < 0$). At (α_c, k_c), $\phi_1(x)$ represents the single neutral mode corresponding to the critical eigenvalue. A dispersion relation is defined at α_c:

$$\omega_c(k) + i\sigma_c(k) = kc, \tag{2.8}$$

where c is the critical eigenvalue. A few properties of this dispersion relation are

$$\sigma_c(k_c) = 0, \quad \frac{\partial\omega_c(k_c)}{\partial k} = c_g, \quad \frac{\partial\sigma_c(k_c)}{\partial k} = 0, \tag{2.9}$$

where c_g is the group velocity. After finding α_c and k_c, the finite-amplitude shear wave behaviour for small values of ϵ is found by setting $\alpha = \alpha_c(1-\epsilon^2)$ so that the perturbation grows slowly. The evolution of the instability is determined at $O(\epsilon^2)$ and $O(\epsilon^3)$.

At $O(\epsilon^2)$, the following scalings are introduced (Stewartson & Stuart 1971; Craik 1985):

$$\tau = \epsilon^2 t, \quad Y = \epsilon(y - c_g t), \tag{2.10}$$

where τ is a slow time, and Y is a stretched alongshore coordinate moving with the group velocity, c_g. The differential operators for time and the alongshore coordinate are replaced by

$$\partial_t \to \partial_t - \epsilon c_g \partial_Y + \epsilon^2\partial_\tau, \quad \partial_y \to \partial_y + \epsilon\partial_Y. \tag{2.11}$$

Again the perturbation streamfunction ψ is expanded in powers of ϵ (2.5), and ψ_1, ψ_2, and ψ_3 have the following forms:

$$\psi_1 = A(\tau, Y)\phi_1(x)\exp[ik_c(y-ct)] + \text{c.c.}, \tag{2.12}$$

$$\psi_2 = AA^*\phi_2^{(0)}(x) + A_Y\phi_2^{(1)}(x)\exp(ik_c(y-ct)) + A^2\phi_2^{(2)}(x)\exp[2ik_c(y-ct)] + \text{c.c.}, \tag{2.13}$$

$$\psi_3 = |A|^2 A\phi_3^{(1)}(x)\exp[ik_c(y-ct)] + \text{c.c.} + \cdots, \tag{2.14}$$

where k_c is the critical wavenumber, c is the phase speed of the neutral wave at (α_c, k_c), and $A(\tau, Y)$ is the amplitude of the shear wave which may have slow variations in the alongshore direction and in time. The term proportional to $\phi_2^{(0)}(x)$ represents the correction to the mean transport, and that proportional to $\phi_2^{(2)}(x)$ the forced harmonic at twice the primary frequency (second harmonic).

Applying the scalings for time and alongshore coordinate (2.11) to the full perturbation equation (2.4) with $\alpha = \alpha_c(1-\epsilon^2)$ and collecting terms of $O(\epsilon)$ and $O(\epsilon^2)$ gives

$$\mathrm{L}_c[\psi_1] = 0,$$

and

$$\begin{aligned} \mathrm{L}_c[\psi_2] = {} & \frac{\psi_{1y}}{x}\left(\nabla^2\psi_{1x} - 2\nabla^2\psi_1/x - \psi_{1xx}/x + 3\psi_{1x}/x^2\right) \\ & -\frac{\psi_{1x}}{x}\left(\nabla^2\psi_{1y} - \psi_{1xy}/x\right) + c_g(\nabla^2\psi_1 - \psi_{1x}/x)_Y \\ & -V(\psi_{1xx} + 3\psi_{1yy} - \psi_{1x}/x)_Y + xQ_x\psi_{1Y} - 2\psi_{1yYt} - \frac{2\alpha_c}{x}\psi_{1yY}, \end{aligned} \tag{2.15}$$

where the linear operator $\mathrm{L}_c[\psi]$ is the operator $\mathrm{L}[\psi]$ defined in (2.6) with $\alpha = \alpha_c$. Substituting (2.12) for ψ_1 and (2.13) for ψ_2 into (2.15) and collecting terms proportional to AA^* yields

$$\begin{aligned} \mathrm{L}_0[\phi_2^{(0)}] = \frac{\alpha_c}{x}\left(\phi_{2xx}^{(0)} - \frac{2\phi_{2x}^{(0)}}{x}\right) = {} & \frac{\mathrm{i}k_c}{x}\left(\phi_1\phi_{1xxx}^* - \phi_{1xxx}\phi_1^* + \phi_{1x}\phi_{1xx}^* - \phi_{1xx}\phi_{1x}^*\right) \\ & + \frac{3\mathrm{i}k_c}{x^2}\left(\phi_{1xx}\phi_1^* - \phi_1\phi_{1xx}^*\right) + \frac{3\mathrm{i}k_c}{x^3}\left(\phi_1\phi_{1x}^* - \phi_{1x}\phi_1^*\right) \end{aligned} \tag{2.16}$$

with the boundary conditions $\phi_2^{(0)} = 0$ at $x = 0$ and $x = \infty$. The linear operator L_0 is L_n (with $n = 0$), where

$$\mathrm{L}_n[\phi] = \mathrm{i}nk_c\left(V - \frac{\mathrm{i}\alpha_c}{nk_cx} - c\right)(\phi_{xx} - \phi_x/x - (nk_c)^2\phi) - \mathrm{i}nk_cxQ_x\phi - \frac{\alpha_c}{x^2}\phi_x \tag{2.17}$$

and n is an integer. The $O(\epsilon^2)$ terms proportional to $A_Y \exp[\mathrm{i}k_c(y - ct)]$ give

$$\begin{aligned} \mathrm{L}_1[\phi_2^{(1)}] = {} & c_g(\phi_{1xx} - \phi_{1x}/x - k_c^2\phi_1) - V(\phi_{1xx} - \phi_{1x}/x - 3k_c^2\phi_1) \\ & + \left(xQ_x - 2k_c^2c - \frac{2\alpha_c\mathrm{i}k_c}{x}\right)\phi_1. \end{aligned} \tag{2.18}$$

In general, $\phi_2^{(1)}$ is resonantly forced since the homogeneous problem, $L_1[\varphi] = 0$, is satisfied with the stated choice of α_c, k_c, and c. The solvability condition for $\phi_2^{(1)}$ requires that c_g satisfy

$$\begin{aligned} c_g\int_0^\infty \phi_1^\dagger(\phi_{1xx} - \phi_{1x}/x - k_c^2\phi_1)\mathrm{d}x = {} & \int_0^\infty \phi_1^\dagger V(\phi_{1xx} - \phi_{1x}/x - 3k_c^2\phi_1)\mathrm{d}x \\ & - \int_0^\infty \phi_1^\dagger\left(xQ_x - 2k_c^2c - \frac{2\alpha_c\mathrm{i}k_c}{x}\right)\phi_1\mathrm{d}x, \end{aligned} \tag{2.19}$$

where $\phi_1^\dagger(x)$ is the adjoint function of $\phi_1(x)$ and is defined in Appendix A. The c_g found by (2.19) should be equal to that found from the dispersion relationship (2.9), providing a useful check of both the algebra and the numerical computations. With c_g (2.18) can be solved for $\phi_2^{(1)}$ subject to boundary conditions $\phi_2^{(1)}(x) = 0$ at $x = 0$ and $x = \infty$. The $O(\epsilon^2)$ terms proportional to $A^2\exp[2\mathrm{i}k_c(y - ct)]$ are

$$\mathrm{L}_2[\phi_2^{(2)}] = \frac{\mathrm{i}k_c}{x}(\phi_1\phi_{xxx} - \phi_{1x}\phi_{1xx}) + \frac{\mathrm{i}k_c}{x^2}\left(-3\phi_1\phi_{1xx} + 2k_c^2\phi_1^2 + \phi_{1x}^2\right) + \frac{3\mathrm{i}k_c}{x^3}(\phi_1\phi_{1x}), \tag{2.20}$$

where L_2 is the operator L_n in (2.17) with $n = 2$. With the boundary conditions, $\phi_2^{(2)} = 0$ at $x = 0$ and $x = \infty$, (2.18) can be solved for $\phi_2^{(2)}(x)$.

The equation for the amplitude $A(\tau, Y)$ of the instability is determined from $O(\epsilon^3)$

terms in (2.4) with $\alpha = \alpha_c(1-\epsilon^2)$,

$$\begin{aligned}
\mathrm{L}[\psi_3] = &-\left(\nabla^2\psi_1 - \frac{\psi_{1x}}{x}\right)_\tau + \frac{\alpha_c}{x}\left(\nabla^2\psi_1 - \frac{2\psi_{1x}}{x}\right) - \frac{\alpha_c}{x}(\psi_{1YY} + 2\psi_{2yY}) \\
&-(\psi_{1YYt} + 2\psi_{2yYt}) + xQ_x\psi_{2Y} + c_g\left(2\psi_{1yYY} + \psi_{2xxY} + \psi_{2yyY} - \frac{\psi_{2xY}}{x}\right) \\
&-V\left(3\psi_{1yYY} + \psi_{2xxY} + 3\psi_{2yyY} - \frac{\psi_{2xY}}{x}\right) \\
&+\frac{\psi_{1y}}{x}\left(\nabla^2\psi_{2x} - \frac{3\psi_{2xx}}{x} - \frac{2\psi_{2yy}}{x} + \frac{3\psi_{2x}}{x^2}\right) \\
&+\frac{\psi_{2y}}{x}\left(\nabla^2\psi_{1x} - \frac{3\psi_{1xx}}{x} - \frac{2\psi_{1yy}}{x} + \frac{3\psi_{1x}}{x^2}\right) \\
&+\frac{\psi_{1Y}}{x}\left(\nabla^2\psi_{1x} - \frac{3\psi_{1xx}}{x} - \frac{2\psi_{1yy}}{x} + \frac{3\psi_{1x}}{x^2}\right) \\
&+\frac{\psi_{1y}}{x}\left(2\psi_{1xyY} - \frac{4\psi_{1yY}}{x}\right) - \frac{\psi_{2x}}{x}\left(\nabla^2\psi_{1y} - \frac{\psi_{1xy}}{x}\right) \\
&-\frac{\psi_{1x}}{x}\left(\nabla^2\psi_{2y} - \frac{\psi_{2xy}}{x}\right) - \frac{\psi_{1x}}{x}\left(\psi_{1xxY} + 3\psi_{1yyY} - \frac{\psi_{1xY}}{x}\right). \qquad (2.21)
\end{aligned}$$

The equation for $A(\tau, Y)$ is derived by substituting (2.12) for ψ_1 and (2.13) for ψ_2, and invoking the solvability condition for ψ_3. The terms on the right-hand side of (2.21) proportional to $\exp[\mathrm{i}k_c(y-ct)]$ are multiplied by the adjoint function $\phi_1^\dagger$ and integrated in the cross-shore direction. The left-hand side is identically zero (A 1) and setting the right-hand side to zero yields a complex Ginzburg–Landau equation for the amplitude of the instability

$$A_\tau = \sigma A + \delta A_{YY} + \mu|A|^2 A, \qquad (2.22)$$

where σ is the growth rate of the disturbance, δ is a dispersion term, and μ is the Landau coefficient which can limit the growth of the disturbance. These coefficients are all complex in general. First κ, which is given by the terms proportional to $A_\tau \exp[\mathrm{i}k_c(y-ct)]$ on the right-hand side of (2.21), is defined

$$\kappa = \int_0^\infty \phi_1^\dagger(\phi_{1xx} - \phi_{1x}/x - k_c^2\phi_1)\,\mathrm{d}x. \qquad (2.23)$$

The growth rate is given by the terms proportional to $A\exp[\mathrm{i}k_c(y-ct)]$ on the right-hand side of (2.21),

$$\sigma\cdot\kappa = \int_0^\infty \phi_1^\dagger\frac{\alpha_c}{x}\left(\phi_{1xx} - 2\phi_{1x}/x - k_c^2\phi_1\right)\mathrm{d}x. \qquad (2.24)$$

The terms proportional to $A_{YY}\exp[\mathrm{i}k_c(y-ct)]$ on the right-hand side of (2.21) define δ,

$$\delta\cdot\kappa = \int_0^\infty \phi_1^\dagger S\,\mathrm{d}x, \qquad (2.25)$$

where

$$\begin{aligned}
S = \left(-\frac{\alpha_c}{x} + \mathrm{i}k_c(c + 2c_g - 3V)\right)\phi_1 + \left(xQ_x - 2\mathrm{i}k_c\frac{\alpha_c}{x} - k_c^2(2c + c_g - 3V)\right)\phi_2^{(1)} \\
+\frac{V - c_g}{x}\phi_{2x}^{(1)} + (c_g - V)\,\phi_{2xx}^{(1)}.
\end{aligned}$$

The terms on the right-hand side of the $O(\epsilon^3)$ equation that are proportional to $|A|^2 A \exp[\mathrm{i}k_c(y-ct)]$ define the complex Landau constant μ,

$$\mu \cdot \kappa = \int_0^\infty \phi_1^\dagger T \,\mathrm{d}x, \tag{2.26}$$

where

$$\begin{aligned} T = {} & \frac{\mathrm{i}k_c}{x}\left[2\phi_1\phi_{2xxx}^{(0)} - \phi_1^*\phi_{2xxx}^{(2)} - 2\phi_{1x}^*\phi_{2xx}^{(2)} + 2\phi_{xxx}^*\phi_2^{(2)} - 2\phi_{1xx}\phi_{2x}^{(0)} + \phi_{1xx}^*\phi_{2x}^{(2)}\right. \\ & \left. + k_c^2(3\phi_1^*\phi_{2x}^{(2)} + 6\phi_{1x}^*\phi_2^{(2)} + 2\phi_1\phi_{2x}^{(0)})\right] \\ & + \frac{\mathrm{i}k_c}{x^2}\left(-6\phi_1\phi_{2xx}^{(0)} + 3\phi_1^*\phi_{2xx}^{(2)} + \phi_{1x}^*\phi_{2x}^{(2)} - 6\phi_{1xx}^*\phi_2^{(2)} + 2\phi_{1x}\phi_{2x}^{(0)} - 4k_c^2\phi_1^*\phi_2^{(2)}\right) \\ & + \frac{\mathrm{i}k_c}{x^3}\left(6\phi_1\phi_{2x}^{(0)} - 3\phi_1^*\phi_{2x}^{(2)} + 6\phi_{1x}^*\phi_2^{(2)}\right). \end{aligned}$$

The complex Ginzburg–Landau equation (2.22) can exhibit a rich behaviour of solutions depending on the values of its coefficients (Manneville 1990). When the real part of the Landau coefficient is negative, finite-amplitude solutions can be found of the form

$$A(\tau, Y) = B\exp[\mathrm{i}(\Lambda Y - \Omega\tau)], \tag{2.27}$$

where B is a complex constant. The simplest solution is when $\Lambda = 0$, and

$$|B|^2 = -\frac{\mathrm{Re}(\sigma)}{\mathrm{Re}(\mu)}, \tag{2.28}$$

$$\Omega = -\left[\mathrm{Im}(\sigma) + |B|^2\mathrm{Im}(\mu)\right]. \tag{2.29}$$

This solution is side-band stable (Benjamin & Feir 1967; Stuart & DiPrima 1978) if

$$\frac{\mathrm{Im}(\mu)\mathrm{Im}(\delta)}{\mathrm{Re}(\mu)\mathrm{Re}(\delta)} + 1 > 0. \tag{2.30}$$

3. Calculations for ANH96 base-state conditions

The beach slope ($\beta = 0.05$) and forcing of ANH96 will be used for the weakly nonlinear calculations. The ANH96 base-state dimensional alongshore velocity is

$$V(x) = C_o x^2 \exp\left(-\frac{x^3}{\delta^3}\right), \tag{3.1}$$

where

$$C_o = 2.404\,609\,9 \times 10^{-4}\frac{1}{\mathrm{m}\times\mathrm{s}}, \quad \delta = 103.02\ \mathrm{m}$$

so that the maximum in V is 1 m s^{-1} and occurs at $x = 90$ m. Therefore the chosen velocity scale is $U = 1$ m s^{-1}. The length scale becomes $L = 90$ m. The ratio $L^3/\delta^3 = 2/3$, and the time scale is $T = 90$ s. The inverse Reynolds number for these scaling choices is $\alpha = 20\nu$. The maximum Froude number is $Fr_{max} = 0.154$, close to the value of 0.14 found to satisfy the rigid-lid approximation for the linear stability problem (Falques & Iranzo 1994). The non-dimensional base-state alongshore velocity $V(x)$ and potential vorticity $Q(x)$ become

$$V(x) = V_o x^2 \exp\left(-2x^3/3\right), \quad V_o = \frac{C_o L^2}{U} = \exp(2/3), \tag{3.2a}$$

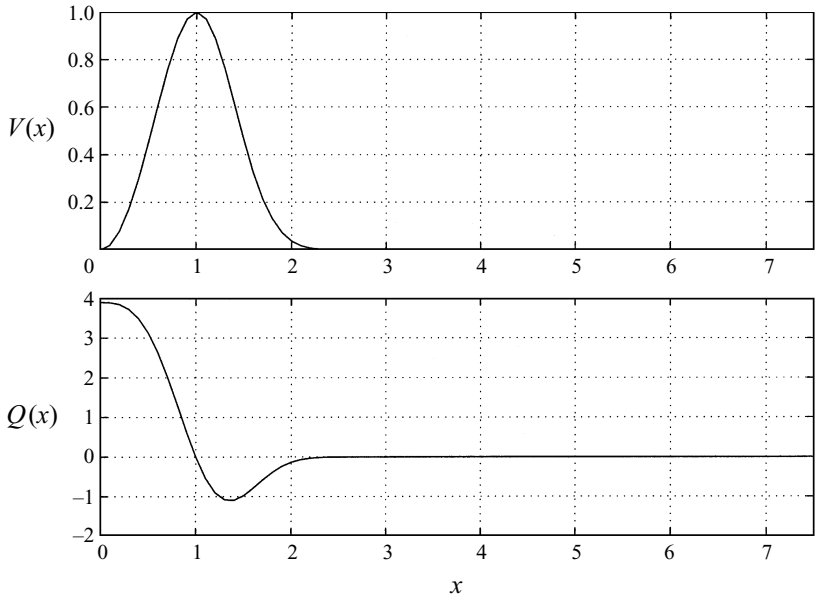

FIGURE 2. The base-state non-dimensional alongshore current $V(x)$ (3.2a) and potential vorticity $Q(x)$ (3.2b).

$$Q(x) = 2V_o(1 - x^3)\exp\left(-2x^3/3\right), \tag{3.2b}$$

and are shown in figure 2. The potential vorticity has a minimum, which satisfies the Rayleigh condition for inviscid instability.

ANH96 used a dimensional domain extending from $x = 0$ to $x = 1000$ m and from $y = 0$ to $y = 450$ m, corresponding to a non-dimensional domain extending to $x = 11.1\overline{11}$ and $y = 5$. Because the solution is expected to decay exponentially offshore (Appendix B) a smaller non-dimensional domain extending to $x = 7.5$ is used here. A second-order finite difference scheme is used with $N-1$ grid points so $\delta x = 7.5/N$. In order to accurately do the weakly nonlinear analysis, α_c, k_c, c, and the eigenfunctions must be precisely known. Therefore, c and ϕ_1 are extrapolated from calculations in extended precision (32 significant digits) on grids with $N-1$, $2N-1$, and $4N-1$ points, giving an accuracy of $O(\delta x^6)$. To find α_c and the dispersion relationship, (2.7) was solved on the three grids using $N = 2500$ ($\delta x = 0.003$) by inverse iteration, which is highly efficient for large tridiagonal systems (Golub & Van Loan 1996). From the solutions on the three grids, c and ϕ_1 are extrapolated giving errors of $O(\delta x^6) = 10^{-16}$. A search was performed in (α, k) space to find the pair of values (α_c, k_c) where one eigenvalue has a zero imaginary component, and all the others have negative imaginary components. For the given beach slope and background velocity, the critical values are $\alpha_c = 0.201\,189\,612\,42$ and $k_c = 1.363\,262\,549\,16$. The eigenvalue spectrum is shown in figure 3(a). The critical eigenvalue is well separated from the other eigenvalues (figure 3b). The adjoint eigenvalue spectrum at α_c and k_c from (A 2) is calculated in the same manner and, as expected, is identical to the eigenvalue spectrum of (2.7). The numerical value of the maximum non-dimensional growth rate at α_c is very close to zero ($\sigma_c(k_c) = k_c c_i = 2 \times 10^{-11}$, corresponding to a dimensional growth time scale of 10^5 years). The points on the dispersion relation (2.8) near k_c are well fitted by a parabola (figure 4, the coefficients of the parabola are given in table 1) indicating that a Taylor series expansion of the dispersion relationship near k_c is

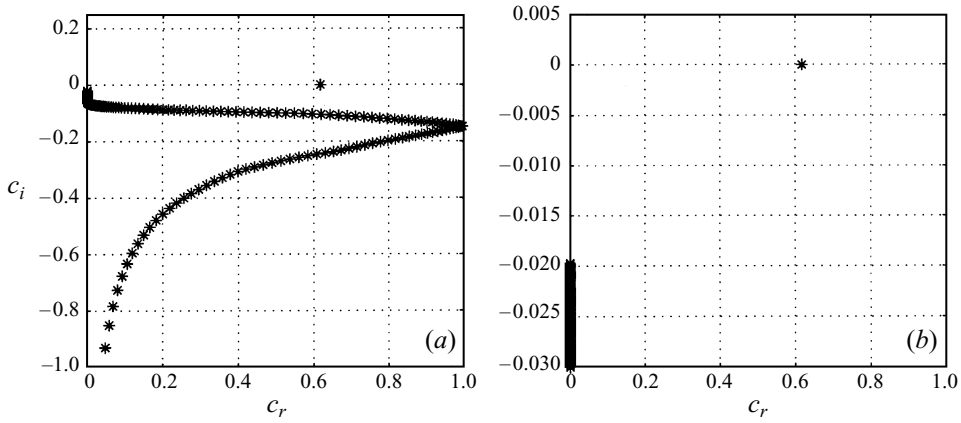

FIGURE 3. (*a*) Real and imaginary parts of the eigenvalues of (2.7) at $\alpha_c = 0.201\,189$ and $k_c = 1.363\,262\,549$, and (*b*) the spectrum enlarged to show the region $-0.030 < c_i < 0.005$.

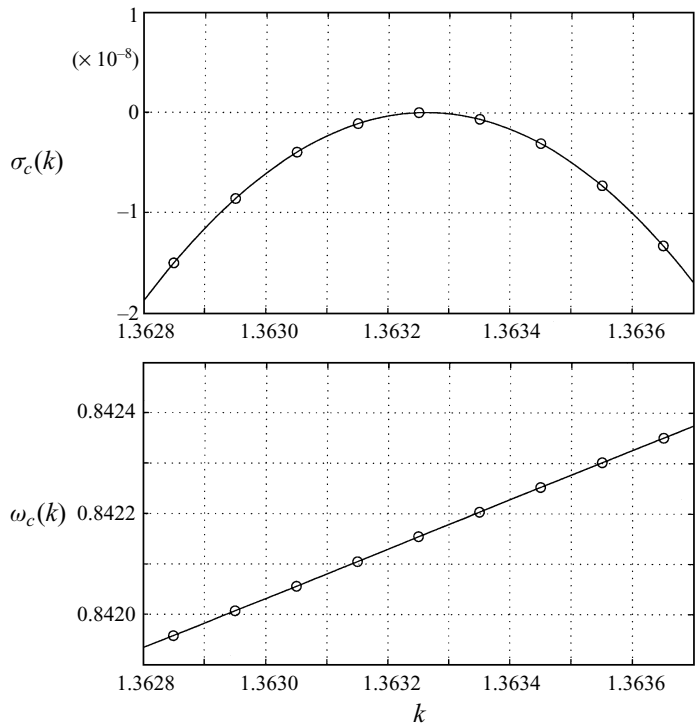

FIGURE 4. The critical dispersion curve for $\omega_c(k) + i\sigma_c(k) = kc$ near the critical wavenumber k. The circles represent calculated values. The solid lines are the best-fit parabolas from the coefficients of table 1.

valid. Based on the coefficients in table 1, the phase speed at the critical wavenumber is $c = 0.617\,753\,649\,7$ and by (2.9) the group velocity is $c_g = 0.490\,600\,164\,4$.

Once the critical frictional parameter and wavenumber are known, ϕ_1 is calculated from (2.7) using α_c and k_c with the same numerical scheme on much denser grids where $N = 10\,000$ ($\delta x = 7.5 \times 10^{-4}$). Denser grids are used because third derivatives must be accurately calculated to find the coefficients of the complex Ginzburg–Landau

	a_2	a_1	a_0
$\omega(k)$	0.012 869 479 738 04	0.490 600 164 421 66	0.842 160 415 251 88
$\sigma(k)$	−0.088 322 793 143 48	0	$1.893\,23 \times 10^{-11}$

TABLE 1. The quadratic coefficients for the growth rate and frequency, $\omega_c(k) + i\sigma_c(k) = a_2(k-k_c)^2 + a_1(k-k_c) + a_0$ where $k_c = 1.363\,262\,549\,16$.

σ	$0.123\,746 - \mathrm{i}0.014\,047$
δ	$0.088\,330 + \mathrm{i}0.012\,854$
μ	$-321.730\,54 + \mathrm{i}407.930\,56$
$\lvert B\rvert$	0.0196 11
Ω	−0.1428 53

TABLE 2. Coefficients for the complex Ginzburg–Landau equation and solution values.

equation. The real and imaginary parts of the normalized and extrapolated ϕ_1 are shown in figure 5(*a*). The adjoint function $\phi_1^\dagger$, shown in figure 5(*b*), is calculated in a similar manner. The group velocity c_g calculated from (2.19), where the derivatives of ϕ_1 and the integrals are extrapolated, yields a value of $c_g = 0.490\,600\,157\,2 - 0.35 \times 10^{-8}\mathrm{i}$. This agrees with the value from the dispersion relationship (2.9) to 10^{-8} in both the real and imaginary parts, serving as a check of the numerical computations. The functions $\phi_2^{(0)}$ and $\phi_2^{(2)}$ (figure 5*c* and figure 5*e*) are calculated from (2.16) and (2.20) on grids identical to those used for ϕ_1 with a standard tridiagonal matrix solver, and extrapolated. The function $\phi_2^{(1)}$ is found by solving (2.18) with a singular value decomposition of the L_1 matrix with $N = 999$ grid points. There is one well-isolated zero (10^{-13}) singular value, and the forward and adjoint null vectors of the L_1 matrix are proportional to ϕ_1 and $\phi_1^\dagger$. The solution for $\phi_2^{(1)}$ (figure 5*d*) is constructed by suppressing the homogeneous solution to L_1. The derivatives of ϕ_1, $\phi_2^{(0)}$, $\phi_2^{(1)}$, $\phi_2^{(2)}$ and the integrals in (2.23), (2.24), (2.26) are extrapolated to derive the coefficients of the complex Ginzburg–Landau equation (2.22), summarized in table 2. The value of δ can also be calculated (Stewartson & Stuart 1971) from the linear dispersion relationship (figure 4 and the dispersion relation coefficients in table 1) by

$$\delta = -\frac{1}{2}\frac{\partial^2 \sigma_c}{\partial k^2} + \mathrm{i}\frac{1}{2}\frac{\partial^2 \omega_c}{\partial k^2}. \tag{3.3}$$

These two estimates of δ agree to three significant digits. The accuracy of the agreement between the two is much smaller than that between the two estimates of c_g (from (2.9) and (2.19)), because δ is calculated from (2.25) where $\phi_2^{(1)}(x)$ is found on a much coarser grid than for example $\phi_1(x)$.

The real part of the Landau coefficient is negative so in this case the instability is supercritical, and finite-amplitude equilibration is possible. A solution for the amplitude of the shear wave is sought that has the form (2.27) with $\Lambda = 0$. The values of B (2.28) and Ω (2.29) are given in table 2. The values of μ and δ are such that this solution for $A(\tau, Y)$ is side-band stable (2.30) for the stated choice of beach slope and base-state alongshore current. For other choices of beach slope and base-state alongshore currents, the instability could be either subcritical or side-band unstable.

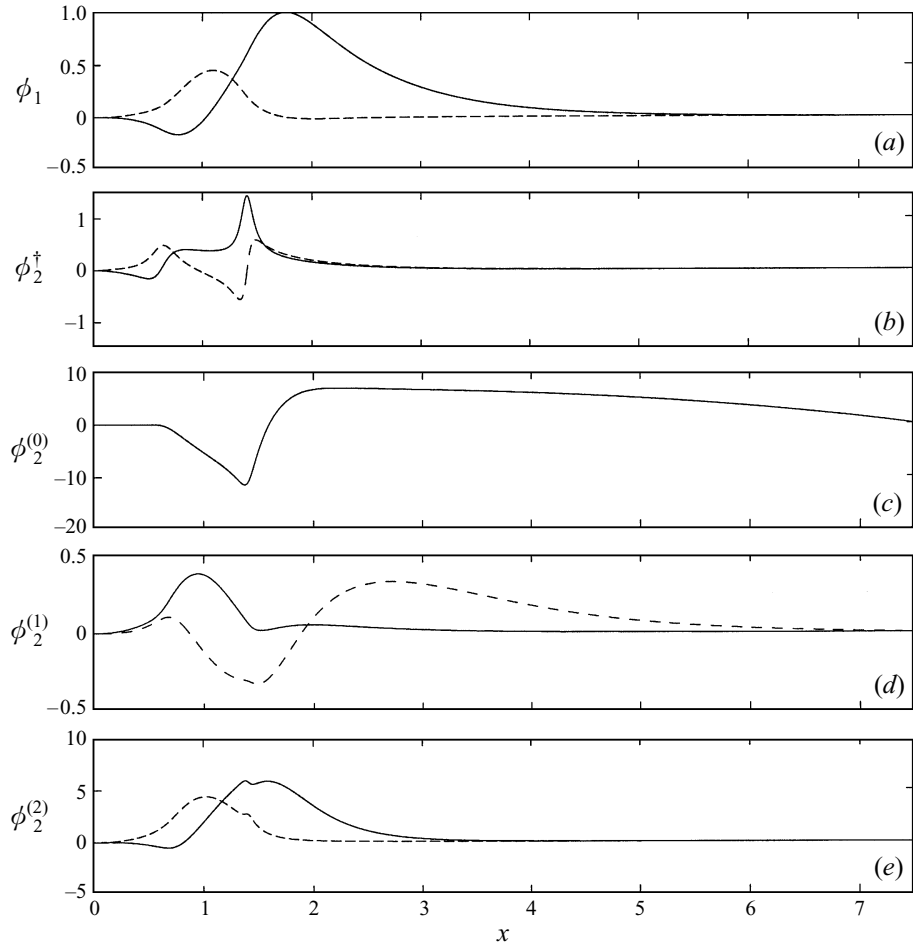

FIGURE 5. The real (solid) and imaginary (dashed) parts of (*a*) ϕ_1, (*b*) $\phi_1^\dagger$, (*c*) $\phi_2^{(0)}$, (*d*) $\phi_2^{(1)}$, and (*e*) $\phi_2^{(2)}$.

4. Analytic and numerical model comparison

Due to numerical limitations, the near critical behaviour of the ANH96 model may be distorted. Therefore, analytic and ANH96 numerical results will be compared for the same non-dimensional beach profile ($h = x$) and base-state alongshore current (3.2*a*) at two values of $\alpha = 0.18$ and 0.17. There are differences between the two models. The ANH96 model is a second-order finite-difference model of essentially the equations (2.1), but also includes weak biharmonic friction ($-\nu_*\nabla^4 u$ and $-\nu_*\nabla^4 v$ added to the right-hand side of (2.1*b*) and (2.1*c*)) to suppress numerical instabilities. Boundary conditions of no flow into the shoreline and offshore boundary are used. Additional boundary conditions ($u_{xx} = v_x = v_{xxx} = 0$) are required at the shoreline and offshore boundary in the ANH96 model due to the fourth-order derivatives in the biharmonic friction terms. The finite-difference representation for biharmonic friction and the associated boundary conditions may influence the development of the instability. ANH96 use a numerical resolution with $N = 200$ grid points in x, $M = 90$ points in y, and a non-dimensional grid spacing $\delta x = \delta y = 0.044$. The

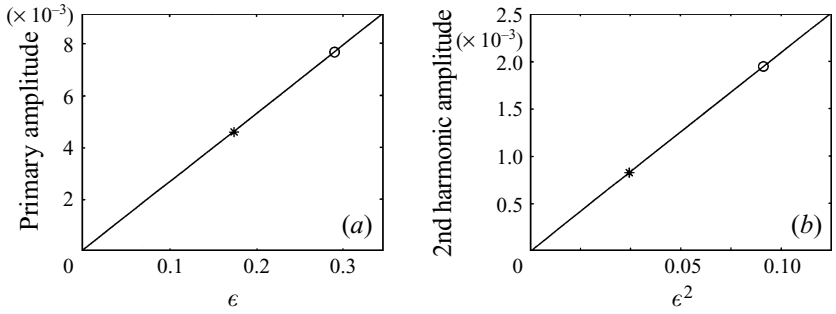

FIGURE 6. (*a*) The ANH96 model peak amplitude at the primary frequency at $x = 1$ versus ϵ for $\alpha = 0.18$ (*) and $\alpha = 0.17$ (○). The inferred $\alpha_c = 0.185\,64$. (*b*) The amplitude of the second harmonic versus ϵ^2. The inferred $\alpha_c = 0.187\,41$.

finite numerical resolution of ANH96 may also mask the near critical behaviour (e.g. Hyman *et al.* 1986).

Periodic boundary conditions are used in the alongshore direction, and the alongshore domain is slightly longer than the wavelength of the theoretical critical wave, leading to a smaller wavenumber ($k = 1.2566$ vs. $k_c = 1.3632$) for the ANH96 critical wave. Therefore the most unstable wave cannot grow, and an evolution of the instability to smaller wavenumbers is restricted. ANH96 also ran numerical experiments with an alongshore domain three times the wavelength of the most unstable mode and stronger nonlinearity ($\alpha \leqslant 0.12$ corresponding to $\epsilon > 0.6$), and reported a shift toward lower frequencies and wavenumbers as the instability evolved. For $\alpha = 0.15$ ($\epsilon \approx 0.45$), more strongly nonlinear than the values of α investigated here, steady equilibrated waves with the same frequencies and wavenumber as the experiments with the smaller domains were reported (figure 7 of ANH96). However, even on the extended alongshore domain, a potential side-band instability of the shear wave is still suppressed. Due to these limitations of the ANH96 model, the near critical behaviour of shear waves may be modelled incorrectly, and for these reasons, the α_c and hence ϵ for the ANH96 model are not accurately known.

Before comparing the results of the ANH96 model with the analytic model, it is first verified that the ANH96 model at $\alpha_c = 0.17$ and $\alpha_c = 0.18$ is in a weakly nonlinear regime. For weakly nonlinear waves, the amplitude at the primary frequency a_1 depends linearly on ϵ and the amplitude at the second harmonic a_2 depends on ϵ^2. Both amplitudes should vanish when $\epsilon = 0$. The α_c is found so that the line going through the (ϵ,a_1) and (ϵ^2,a_2) points have zero y-intercept (figure 6). The resulting estimates of α_c are quite similar, $\alpha_c = 0.185\,64$ from the primary frequency and $\alpha_c = 0.18741$ from the second harmonic, confirming the ANH96 model is in a weakly nonlinear regime. Using $\alpha_c = 0.185\,64$, $\epsilon = 0.174$ for $\alpha = 0.18$ and $\epsilon = 0.290$ for $\alpha = 0.17$.

The choice of α_c feeds back into all parts of the solution to the weakly nonlinear problem, so it is not possible to use the ANH96-derived α_c to compare results from the ANH96 and analytic models. Therefore, the analytic $\alpha_c = 0.20119$ is used to calculate ϵ for comparison purposes, resulting in $\epsilon = 0.325$ for $\alpha = 0.18$ and $\epsilon = 0.394$ for $\alpha = 0.17$. As will be shown, this leads to reasonable agreement between analytic and ANH96 model amplitudes for the shear waves, and very good agreement for the cross-shore structure of the shear waves.

The spectrum of ANH96 cross-shore velocity at both values of α contains distinct

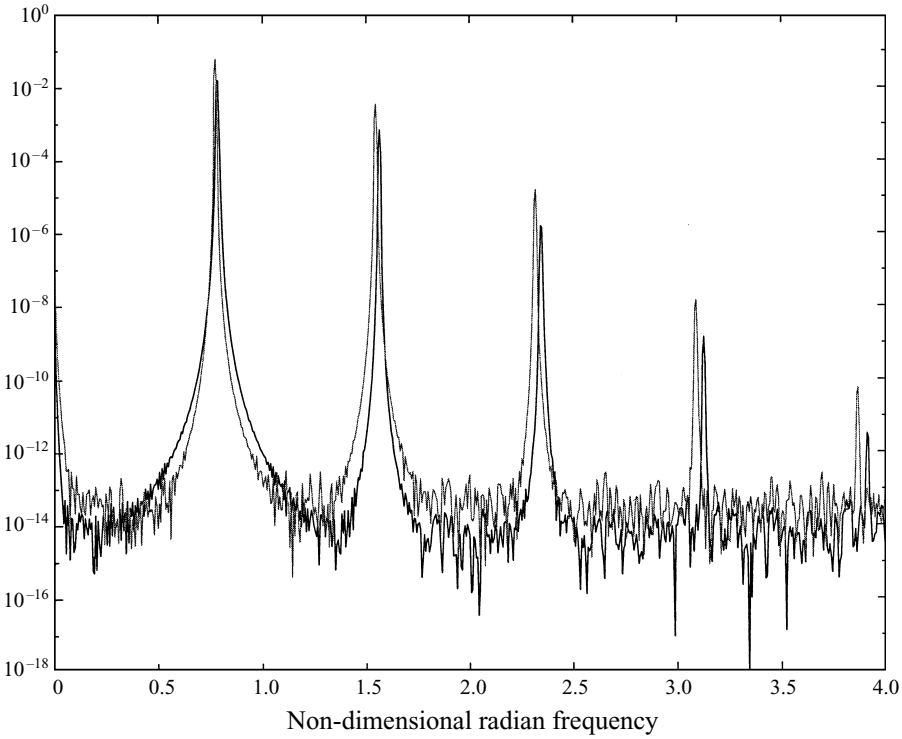

FIGURE 7. Non-dimensional spectra of u at $x = 1$ from ANH96 model with $\alpha = 0.17$ (grey line) and 0.18 (bold line).

peaks at integer multiples of the primary frequency (figure 7). The primary peak in the spectrum at the weakest nonlinearity ($\alpha = 0.18$) has a dimensional period of 12 minutes. The ANH96 model non-dimensional primary frequency $\omega_1 = 0.7822$ is close to the analytical model value $\omega = 0.8421$ at α_c and k_c from linear stability theory (2.7). The difference in frequencies is largely attributable to the ANH96 alongshore domain being slightly longer than the critical wavelength. From (2.7), the smaller wavenumber forced by the domain size corresponds to a frequency $\omega = 0.7899$, close to the ANH96 primary frequency $\omega_1 = 0.7822$.

The shift to lower frequency in the spectral peaks with decreasing α (figure 7) is consistent with amplitude dispersion. The equilibrated cross-shore velocity at the primary frequency and at a fixed alongshore position is

$$u = \frac{-\epsilon \mathrm{i}k}{x}\left(B\phi_1(x)\mathrm{e}^{-\mathrm{i}(\omega_c+\epsilon^2\Omega)t} - B^*\phi_1^*(x)\mathrm{e}^{\mathrm{i}(\omega_c+\epsilon^2\Omega)t}\right) \tag{4.1}$$

indicating a finite-amplitude shift of $\epsilon^2\Omega$ in the primary frequency, where Ω is given by (2.29). At the nth harmonic (e.g. $n\omega_1$) the leading-order frequency shift is given by $n\epsilon^2\Omega$. Therefore the difference in spectral peak frequencies at $\alpha = 0.18$ and $\alpha = 0.17$ is theoretically $n\Delta\epsilon^2\Omega$, where $\Delta\epsilon^2 = (0.18 - 0.17)/\alpha_c$. The ANH96 observed frequency shift for the first four harmonics at the nth harmonic is n times the primary frequency shift (figure 8), consistent with $O(\epsilon^2)$ amplitude dispersion. However, the magnitude of the ANH96 observed frequency shift is about 30% larger than the analytical model frequency shift.

The equilibrated cross-shore velocity of the ANH96 model at a fixed alongshore

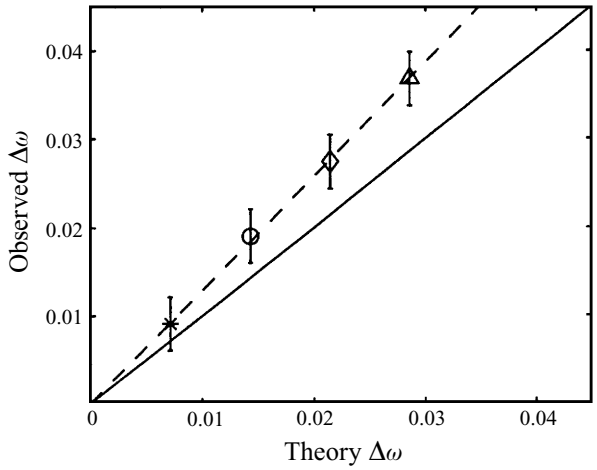

FIGURE 8. The ANH96-derived versus the theoretical change in peak frequency between $\alpha = 0.18$ and $\alpha = 0.17$. Results for the primary frequency (*), second (○), third (◇), and fourth (△) harmonic are shown with $\alpha_c = 0.201\,19$. The error bars (± 0.003) indicate the frequency resolution of the spectrum. The solid line represents perfect ANH96 model–theory agreement. The dashed line is the best fit through the symbols.

position is

$$u(x,t) = U_1(x)\mathrm{e}^{\mathrm{i}\omega_1 t} + U_2(x)\mathrm{e}^{\mathrm{i}2\omega_1 t} + \text{c.c.} + \cdots, \tag{4.2}$$

where ω_1 is the primary wave frequency, and $U_1(x)$ and $U_2(x)$ are the Fourier transforms of the ANH96 cross-shore velocities at ω_1 and $2\omega_1$. $U_1(x)$ and $U_2(x)$ are related to the analytic model by

$$U_1(x) = \frac{-\epsilon B^* \mathrm{i}k\phi_1^*(x)}{x} \quad U_2(x) = \frac{-\epsilon^2 B^{*2} 2\mathrm{i}k\phi_2^{(2)*}(x)}{x}. \tag{4.3a,b}$$

The functions $\phi_1(x)$ and $\phi_2^{(2)}(x)$ can therefore be inferred from the ANH96 cross-shore velocity for $\alpha = 0.18$ and $\alpha = 0.17$. The magnitudes of $|\phi_1(x)|$ and $|\phi_2^{(2)}(x)|$ are equal to the square root of the spectrum of u (e.g. figure 7) summed over a small window of frequencies centred on the primary or secondary frequency (to account for spectral leakage) and multiplied by $x/(\epsilon|B|k)$ or $x/(2\epsilon^2|B|^2k)$ respectively. The phases of $\phi_1(x)$ and $\phi_2^{(2)}(x)$ are given within arbitrary constants from the phases of $U_1(x)$ or $U_2(x)$.

Analytic and ANH96 model solutions for $\phi_1(x)$ and for $\phi_2^{(2)}(x)$ are shown in figures 9 and 10. The magnitudes of the ANH96-derived $\phi_1(x)$ are in approximate agreement with theory (figure 9*a*) using the ϵ derived from the analytic α_c. However, when normalized to the same maximum magnitude, the cross-shore structure of both the ANH96-inferred and theoretical $|\phi_1(x)|$ and $|\phi_2^{(2)}(x)|$ are in very good agreement for both values of α (figures 9*b* and 10*a*). The cross-shore phase structure is also in excellent agreement (figure 9*c* and figure 10*b*), except near the shoreline where the differences are evidently due to the additional boundary conditions applied to the ANH96 model at the shoreline and the resulting boundary layer from the biharmonic friction. Far offshore ($x > 4$), the phase for $\phi_2^{(2)}(x)$ is in error because the signal is so weak.

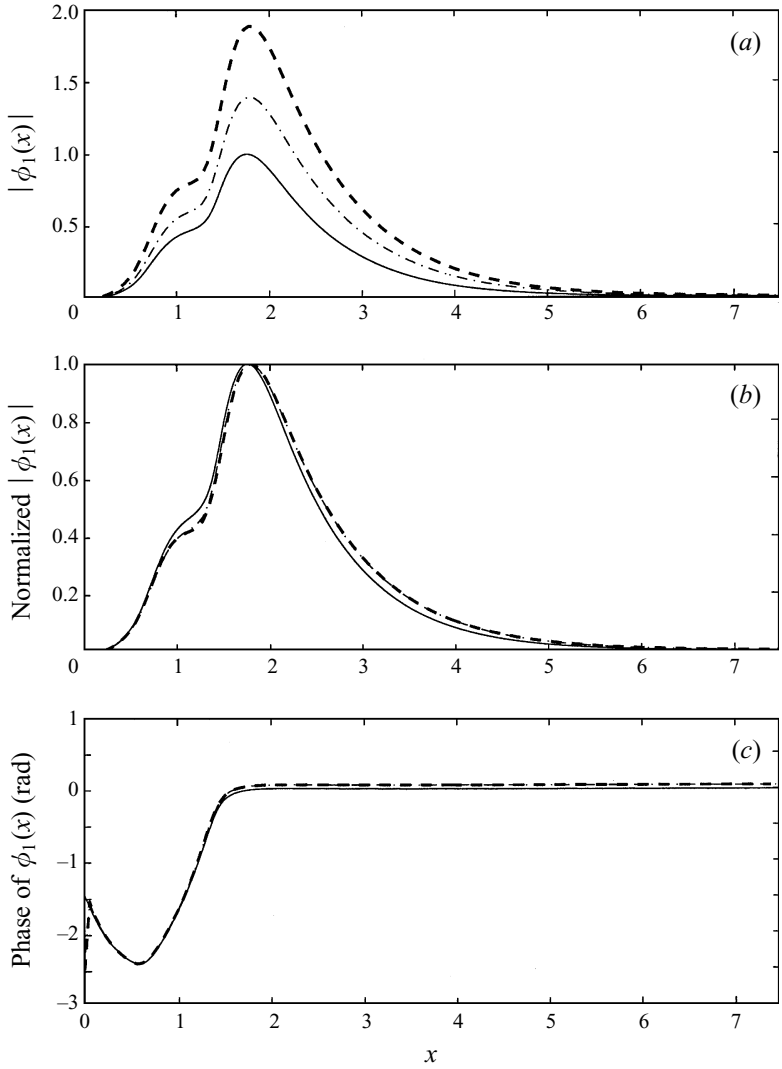

FIGURE 9. (*a*) $|\phi_1(x)|$ versus non-dimensional cross-shore coordinate, x. (*b*) $|\phi_1(x)|$ normalized (to a maximum magnitude of 1.0) versus x. (*c*) The phase of $\phi_1(x)$ versus x. In each panel, theory is a solid line, and ANH96 model $\phi_1(x)$ are inferred with $\alpha_c = 0.20119$, and are shown with $\alpha = 0.18$ (dash-dot) and $\alpha = 0.17$ (dashed). The phases are offset so that they are equal at $x = 0.582$.

The analytic model predicts a mean second-order correction $V_c(x)$ to the alongshore current

$$V_c(x) = \frac{\epsilon^2 |B|^2 \phi_{2x}^{(0)}}{x}. \tag{4.4}$$

The ANH96 correction, defined as the difference between the time mean from the base-state alongshore current $\bar{v}(x) - V(x)$, was calculated for both α. The ϵ^2-normalized theoretical correction to the alongshore current, $V_c/\epsilon^2 = |B|^2 \phi_{2x}^{(0)}/x$, and the ANH96 correction $(\bar{v} - V)/\epsilon^2$ normalized to the same magnitude are also in very good agreement (figure 11). The differences in the correction near the shoreline are again due to the additional boundary conditions applied there. The effect of the mean flow correction is to reduce the offshore velocity shear by decreasing the velocity at the maximum near $x = 1$ and increasing the velocity further offshore.

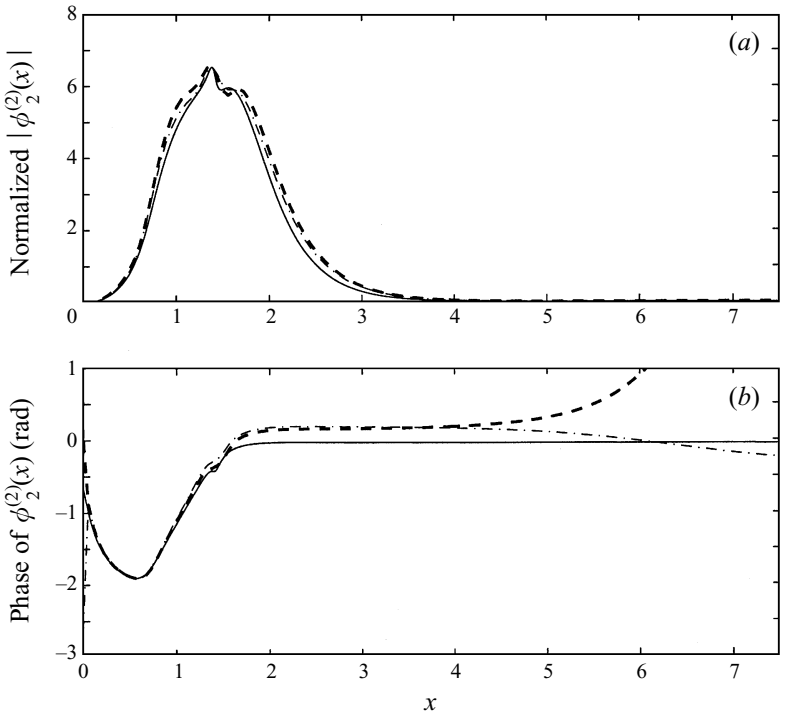

FIGURE 10. (*a*) $|\phi_2^{(2)}(x)|$ normalized (to the maximum theory magnitude) versus x. (*b*) The phase of $\phi_2^{(2)}(x)$ versus x. In each panel theory (solid) and ANH96 model for $\alpha = 0.18$ (dash-dot) and $\alpha = 0.17$ (dashed) are shown. The phases are offset so that they are equal at $x = 0.561$.

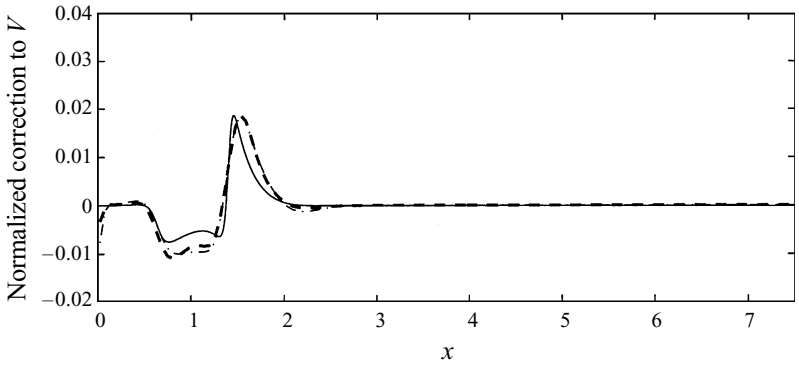

FIGURE 11. The normalized (to have the same maximum magnitude) correction to the mean alongshore current from theory (solid) and ANH96 model for $\alpha = 0.18$ (dash-dot) and $\alpha = 0.17$ (dashed).

5. Discussion and conclusions

Weakly nonlinear shear waves are shown to have characteristics of many other weakly nonlinear wave systems. A standard perturbation expansion is used where the small parameter ϵ is the normalized departure of an inverse Reynolds number α from neutral stability. At $O(\epsilon)$ there is a primary wave with wavenumber k_c, frequency ω_c, and cross-shore structure $\phi_1(x)$ predicted from linear stability theory (e.g. Bowen & Holman 1989; Dodd *et al.* 1992). At $O(\epsilon^2)$, a forced wave at twice

the frequency and wavenumber ($2\omega_c$, $2k_c$) (second harmonic) and a correction to the mean alongshore current are found. At $O(\epsilon^3)$, a complex Ginzburg–Landau equation (2.22) is derived for the amplitude of the shear wave. This derivation is applicable to an alongshore homogeneous planar beach with arbitrary slope and any prescribed alongshore forcing or base-state alongshore current. For the same base-state alongshore current (3.2*a*) and beach slope used in the numerical study of ANH96, the instability is supercritical, and the analytic solution is a side-band stable equilibrated shear wave, with an amplitude-dependent dispersion relationship. Previous work (Dodd *et al.* 1992; Putrevu & Svendsen 1992; Slinn *et al.* 1998) suggests that the shear instability is enhanced by a barred-beach profile. The weakly nonlinear analysis can be in principal extended to non-planar beach profiles; however, the character of the instability may be different from the case presented here.

The near critical behaviour of shear waves in the ANH96 model may be distorted by numerical effects. Biharmonic friction terms added to prevent numerical instabilities and finite model resolution may alter the character of the instability. Waves longer than the primary wavenumber are suppressed due to finite domain lengths, therefore a potential sideband instability cannot develop. Numerical limitations also complicate comparison of the analytic to the ANH96 numerical model. However, the ANH96 model at $\alpha = 0.17$ and $\alpha = 0.18$ is shown to be in a weakly nonlinear regime, and the dominant variability is an equilibrated shear wave with the frequency, wavenumber, and cross-shore structure predicted by linear stability theory. The variability at twice the primary frequency is the second harmonic with the same cross-shore structure as the analytical model. The cross-shore structure of the correction to the mean flow is also in good agreement. Using the analytic α_c, the ANH96 and analytic model shear wave amplitudes are in reasonable agreement, as is the amplitude dispersion. The agreement with the analytical model and ANH96 confirms that the ANH96 model correctly reproduces the qualitative behaviour of the weakly nonlinear shear waves for this choice of beach slope and base-state alongshore current.

The numerical modelling of ANH96 and Slinn *et al.* (1998), and the observational work of Dodd *et al.* (1992) suggest a wide range of possible shear wave environments in natural surf zones, ranging from linearly stable equilibrated shear waves, to strongly turbulent eddy-dominated regimes. Determining whether weakly nonlinear shear waves exist in natural surf zones is beyond the scope of this study. However, the ANH96 base-state alongshore current (3.1) and beach slope ($\beta = 0.05$) from §3 are not completely unrealistic parameters for a natural surf zone. With these parameters, the critical inverse Reynolds number $\alpha_c = 0.201\,19$ leads to a dimensional critical drag coefficient of $\nu_c = 0.01$ m s^{-1}. In the idealized bottom stress representation used here, ν can be thought to represent $\nu = c_f \sigma_u$ where c_f is an empirical drag coefficient and σ_u^2 is the orbital wave velocity variance (Dodd *et al.* 1992; Slinn *et al.* 1998). Using a cited range of c_f in the surf zone from 0.01 to 0.001 (e.g. Garcez Faria *et al.* 1998) and a significant wave height $H_{sig} = 1$ m in 2 m water depth with linear surface gravity wave theory which gives $\sigma_u \approx 0.8$ m s^{-1}, yields a plausible range of ν from 0.008 to 0.0008 m s^{-1}. Given the caveats that the bottom stress representations is crude and the forcing idealized, it appears that the value of $\nu_c = 0.01$ m s^{-1} required for stability in this hypothetical case is not entirely unrealistic for natural surf zones, and also suggests that a natural surf zone could possibly be in a linearly stable or in a weakly nonlinear regime.

Shear wave energy in field data (e.g. Oltman-Shay *et al.* 1989; Dodd *et al.* 1992), appears as an approximately dispersionless band in frequency–wavenumber spectra. Beyond this, little is known about the characteristics of shear waves in natural surf

zones. Future analyses and observations may better characterize surf zone shear wave environments. If shear waves are weakly nonlinear equilibrated linear modes, this might be elucidated with bispectral analysis (e.g. Elgar & Guza 1985) because in the weakly nonlinear limit, the wave at 2ω and $2k$ is bound to the primary wave at ω and k. Future theoretical and observational study could include investigating possible resonances between modes, either leading to explosive instabilities (Shrira *et al.* 1997) or a coupled set of amplitude equations.

Funding for this study was provided by ONR Coastal Sciences and AASert programs, and California Sea Grant. The author appreciates the help of by John Allen and Priscilla Newberger in providing ouput from their model. Glenn Ierley and Bob Guza provided sage advice on many occasions, and Paola Cessi taught the class that inspired this work.

Appendix A. The adjoint operator

The adjoint operator, $\mathrm{L}_1^\dagger$ and the adjoint function $\phi_1^\dagger$ to the linear operator L_1 are defined as

$$\int_0^\infty \phi_1^\dagger \mathrm{L}_1[\phi_1]\mathrm{d}x = \int_0^\infty \phi_1 \mathrm{L}_1^\dagger[\phi_1^\dagger]\mathrm{d}x = 0 \tag{A 1}$$

with $\mathrm{L}_1[\phi_1]$ given by (2.17) with $n = 1$ and and the boundary conditions, $\phi_1 = 0$ at $x = 0$ and $x = \infty$. Integrating by parts yields

$$\mathrm{L}^\dagger[\phi_1^\dagger] = \left(V - \frac{\mathrm{i}\alpha_c}{k_c x} - c\right)\phi_{1xx}^\dagger + \left(2V_x + \frac{V}{x} - \frac{c}{x}\right)\phi_{1x}^\dagger - \left(xQ_x - \frac{\mathrm{i}\alpha_c}{k_c x}\left(k_c^2 + \frac{2}{x^2}\right)\right.$$
$$\left. + V\left(k_c^2 + \frac{1}{x^2}\right) - \frac{V_x}{x} - V_{xx} - c\left(k_c^2 + \frac{1}{x^2}\right)\right)\phi_1^\dagger = 0, \tag{A 2}$$

with the boundary conditions $\phi_1^\dagger = 0$ at $x = 0$ and ∞. The adjoint $\phi_1^\dagger$ is solved at the critical wavenumber, k_c and critical friction parameter, α_c. The adjoint operator $\mathrm{L}^\dagger$ must and does have the same eigenvalue spectrum as the linear operator L_1.

Appendix B. Asymptotics

The asymptotic nature of the linear eigenvalue problem near the beach ($x = 0$) is examined where the dimensional water depth, $h \to 0$. The solution of the linear eigenvalue problem should be analytic near the shoreline and match the prescribed boundary condition, $\phi_1 = 0$. The non-dimensional velocity used by ANH96 (3.2*a*) and resulting potential vorticity gradient are expanded around $x = 0$. The stability equation (2.7) is rewritten as

$$\phi_{1xx} - \frac{\phi_{1x}}{x} - k^2\phi_1 = \frac{\left(Q_o x^3\phi_1 - \frac{\mathrm{i}\alpha}{kx^2}\phi_{1x}\right)\left(V_o x^2 - c + \frac{\mathrm{i}\alpha}{kx}\right)}{\left(V_o x^2 - c - \frac{\mathrm{i}\alpha}{kx}\right)\left(V_o x^2 - c + \frac{\mathrm{i}\alpha}{kx}\right)}$$
$$= \lambda_1(x)\phi_1 + \mathrm{i}\lambda_2(x)\phi_{1x} + \phi_{1x}/x,$$

where $\lambda_1(x)$ and $\lambda_2(x)$ are analytic functions near $x = 0$. The origin is a regular singular point. Expanding in a Frobenius series, the indicial exponents are 0 and 3. The latter gives a non-singular solution that satisfies the boundary condition, $\phi_1(0) = 0$.

The asymptotic behaviour as $x \to \infty$ is also of interest because the solution for

ϕ_1 should match the boundary condition of $\phi_1(\infty) = 0$, in checking the numerical solution for ϕ_1 and helping to choose the proper numerical domain. As $x \to \infty$, terms that are proportional to V and Q_x can be ignored since both have leading-order behaviour $\exp(-2x^3/3)$. The equation becomes

$$\left(c + \frac{\mathrm{i}\alpha}{kx}\right)\phi_{1xx} - \left(c + \frac{2\mathrm{i}\alpha}{kx}\right)\frac{\phi_{1x}}{x} - \left(c + \frac{\mathrm{i}\alpha}{kx}\right)k^2\phi_1 = 0,$$

which has an irregular singular point at $x = \infty$. Substituting $\phi_1 = \mathrm{e}^{S(x)}$, standard asymptotic methods are used to determine that to leading order $S \sim -kx + 1/2 \ln x$ thus

$$\phi_1 \sim x^{1/2}\exp(-kx).$$

Note that this leading order result is independent of both the eigenvalue c and α.

REFERENCES

Allen, J. S., Newberger P. A. & Holman R. A. 1996 Nonlinear shear instabilities of alongshore currents on plane beaches. *J. Fluid Mech.* **310**, 181–213 (referred to herein as ANH96).

Benjamin, T. B. & Feir, J. E. 1967 The disintegration of wave trains on deep water. *J. Fluid Mech.* **27**, 417–430.

Bowen, A. J. & Holman, R. A. 1989 Shear instabilities of the mean longshore current, 1. Theory. *J. Geophys. Res.* **94**, 18023–18030.

Craik, A. D. D. 1989 *Wave Interactions and Fluid Flows.* Cambridge University Press.

Dodd, N., Oltman-Shay, J. & Thornton, E. B. 1992 Shear instabilities in the longshore current: a comparison of observation and theory. *J. Phys. Oceanogr.* **22**, 62–82.

Dodd, N. & Thornton, E. B. 1992 Longshore current instabilities: growth to finite amplitude. *Proc. 23rd Intl Conf. Coastal Engng*, pp. 2644–2668. ASCE.

Elgar, S. & Guza, R. T. 1985 Observations of bispectra of shoaling surface gravity waves. *J. Fluid Mech.* **161**, 425–448.

Falques, A. & Iranzo, V. 1994 Numerical simulation of vorticity waves in the nearshore. *J. Geophys. Res.* **99**, 825–841.

Garcez Faria, A. F., Thornton, E. B., Stanton, T. P., Soares, C. M. & Lippmann, T. C. 1998 Vertical profiles of longshore currents and related bed shear stress and bottom roughness. *J. Geophys. Res.* **103**, 3217–3232.

Golub, G. H. & Van Loan, C. F. 1996 *Matrix Computations*, 3rd edn. Johns Hopkins University Press.

Hyman, J. M., Nicolaenko, B. & Zaleski, S. 1986 Order and complexity in the Kuramoto-Sivashinsky model of weakly turbulent interfaces. *Physica* D **23**, 265–292.

Manneville, P. 1990 *Dissipative Structures and Weak Turbulence.* Academic Press.

Oltman-Shay, J., Howd, P. A. & Birkemeier, W. A. 1989 Shear instabilities of the mean longshore current, 2. Field data. *J. Geophys. Res.* **94**, 18,031–18042.

Özkan, H. T. & Kirby, J. T. 1995 Finite amplitude shear wave instabilities. *Proc. Coastal Dynamics 1995*, pp. 465–476. ASCE.

Putrevu, U. & Svendsen, I. A. 1992 Shear instability of longshore currents: A numerical study. *J. Geophys. Res.* **97**, 7283–7302.

Shrira, V. I., Voronovich, V. V. & Kozhelupova, N. G. 1997 Explosive instability of vorticity waves. *J. Phys. Oceanogr.* **27**, 542–554.

Slinn, D. N., Allen, J. S., Newberger, P. A. & Holman, R. A. 1998 Nonlinear shear instabilities of alongshore currents over barred beaches. *J. Geophys. Res.* (in press).

Stewartson, K. & Stuart, J. T. 1971 A non-linear instability theory for a wave system in plane Poiseulle flow. *J. Fluid Mech.* **48**, 529–545.

Stuart, J. T. & DiPrima, R. C. 1978 The Eckhaus and Benjamin-Feir resonance mechanisms. *Proc. R. Soc. Lond.* A **362**, 27–41.

Thornton, E. B. & Guza, R. T. 1986 Surf zone longshore currents and random waves: field data and models. *J. Phys. Oceanogr.* **16**, 1165–1178.